JOURNAL OF COMPUTATIONAL PHYSICS 112, 126–137 (1994)

Exact and Approximate Riemann Solvers for Real Gases

RICHARD SAUREL, MICHEL LARINI, AND JEAN CLAUDE LORAUD

IUSTI CNRS URA 1168, Universite de Provence, Avenue Escadrille Normandie Niemen, Marseille Cedex 20, France

Received July 29, 1992; revised March 10, 1993

A procedure is developed for solving the Riemann problem (RP) for the flow of gases obeying an equation of state (EOS) of the form $p = p(\rho, T)$. A first method is introduced, producing solutions of the exact RP; the algorithm is validated by applying it to the classical test case of the shock-tube, for a perfect gas. Thereafter, the method is applied to gases having EOS of the Van der Waals or virial types, with very good resulting accuracy; however, the procedure is somewhat demanding in computer time. Therefore, some simplifying assumptions are introduced into the computation of simple waves, leading to an approximate solution of the RP; in most circumstances, excellent results are obtained, and the computer time is much more competitive. However, under certain extreme flow conditions, it is recommended that a combination of the exact and approximate solvers for the RP be employed.

1. INTRODUCTION

Numerical computation methods based upon the Riemann problem (RP) have seen a marked favour during the last decade, mainly through the emergence of high-resolution upwind methods, which make use of the basic concepts introduced by Godunov [7] and Van Leer [20]. The finite-volume formulation of these methods, adapted to computations by unstructured grids, has led to the development of powerful codes, which have allowed us to solve a number of problems involving complex geometrical features.

Solving the RP furnishes a very accurate estimation of the Euler fluxes and, thereby, a high precision in the solution of the gas-dynamic equations. Especially, second-order extensions of Godunov-type schemes, as well as the emergence of TVD (total variation diminishing) algorithms have brought about the possibility to capture the discontinuities with very good accuracy. Last, the formulation of any type of boundary conditions is quite easy, once a Riemann solver is employed for the computation of corresponding points.

More recently, the problems related to the reentry of space vehicles, as well as the development of novel propulsion devices, such as the "Ram Accelerator" have brought into the forefront the need for solving the RP for real gases having an equation of state (EOS) of a general form. However, taking into account the real-gas EOS renders difficult the resolution of the RP. Actually, in the case of a perfect gas, and for a simple wave, there are two Riemann invariants, which may be explicitly expressed in terms of the flow variables:

$$\psi^{\pm}_{GP} = v \mp \frac{2}{\gamma_{pg} - 1} c.$$

Concerning the shock conditions, again in the case of a perfect gas, the shock Mach number is expressed as a function of the pressure ratio, while the other parameters behind the shock may be deduced analytically in terms of the shock Mach number. Therefore, in the case of a perfect gas, all the above-mentioned relations, which connect explicitly the flow parameters between themselves, lead to an easy resolution of the RP [7, 9]. On the contrary, in the case of a real-gas EOS, in a simple wave, as will be discussed hereafter, one has to employ the direct expression of the Riemann invariants:

$$\psi^{\pm} = v \mp \int^{\rho} \tilde{\rho}^{-1} c(\tilde{\rho}, s)\, d\tilde{\rho}$$

and the trouble arises because the integral has to be evaluated along an isentrope curve. Then, for the computation of the state behind a shock wave, the whole coupled jump conditions have to be satisfied simultaneously; thus, the resolution of the RP becomes more involved and demanding in terms of CPU time.

It is, therefore, precisely the problem of solving the RP in the case of a real-gas EOS, that is the subject of the present paper. In this connection, one should recall the work of Toro [19], who solved the RP for an EOS with constant covolume. However, in this case, the Riemann invariants had an analytical expression and, therefore, the resolution procedure was similar to that for a perfect gas. Plohr [16] solved the RP for an EOS of a "stiffened gas," which was supposed to mimic the behaviour of a metallic solid, when traversed by a shock. Here also, the form of EOS allows a

0021-9991/94 $6.00

solution of the type "perfect gas" for the RP. In another approach, one finds in the literature the papers by Liou *et al.* [13] and by Vinokur and Montagné [21], who adapted the flux vector splitting procedure due to Van Leer [20], or the work of Glaister [5], who applied to a real gas the idea of a linearised Riemann solver, due to Roe [17], or, finally, the approximate method by Collela and Glaz [3]. It should be pointed out that Van Leer's method, as well as Roe's, employ approximate solvers for the RP. Such methods are efficient within the framework of a multi-dimensional code, since the approximate solution of the RP is less costly in terms of CPU time. On the other hand, they fail to provide an accurate evaluation of the Eulerian fluxes, as is possible with a method based upon an exact solution of the RP and, as a consequence, they lose precision in the capture of contact surfaces, as well as in the treatment of boundary points.

For these reasons, we felt it was important, first, to be able to provide exact solutions to the RP in the case of a real gas. We propose several techniques of resolution, and we then implement them in the random choice method [6, 4, 8], which is, itself, one of the methods where the RP is implied in a natural way.

In the second section, the principle of an exact numerical method for the RP will be developed for the case of an EOS having the general form $p = p(\rho, T)$. Our approach will be tested upon the classical case of the shock tube, successively for the perfect gas EOS, the Van der Waals EOS, and a fifth-order virial EOS.

In the third part, we dwell upon the necessary assumptions for an approximate solution of the exact Riemann problem; these assumptions concern the Gruneisen coefficient and the adiabatic exponent. Their adoption renders possible a faster numerical computation, as the Riemann invariants take a simple analytic expression of the perfect-gas type. The new procedure will be submitted to the same tests as above. In certain circumstances, under severe thermodynamic conditions, the approximate solution of the RP might be slightly in error; it shall be proposed then to combine the exact solver, applied to questionable points, with the approximate solver, applied to the rest of the flowfield.

2. THE EXACT RIEMANN SOLVER

The one-dimensional Euler equations, in the variables ρ, v, and s (density, velocity, and entropy) may be written as

$$\begin{aligned} &\frac{\partial \rho}{\partial t} + v\frac{\partial \rho}{\partial x} + \rho\frac{\partial v}{\partial x} = 0 \\ &\frac{\partial v}{\partial t} + v\frac{\partial v}{\partial x} + \Gamma T\frac{\partial s}{\partial x} + \frac{c^2}{\rho}\frac{\partial \rho}{\partial x} = 0 \\ &\frac{\partial s}{\partial t} + v\frac{\partial s}{\partial x} = 0. \end{aligned} \tag{1}$$

Here c and Γ are, respectively, the speed of sound and the Gruneisen coefficient, and they are defined as

$$c^2 = \left(\frac{\partial p}{\partial \rho}\right)_s \tag{2}$$

$$\Gamma = \frac{1}{\rho}\left(\frac{\partial p}{\partial e}\right)_\rho = \frac{\rho}{T}\left(\frac{\partial T}{\partial \rho}\right)_s. \tag{3}$$

The choice of the formulation (1) for the Euler equations will allow us to manipulate a system of three equations with three unknowns, without having to specify explicitly the EOS which will be employed. The equation of state is, actually, only necessary for the computation of the sound speed and of the Gruneisen coefficient.

Riemann's viewpoint consists in assuming that, at every point within the flowfield, any variation will engender a couple of waves, facing respectively to the right and to the left. The connection between the two domains (l^*, r^*) takes place across a constant surface. The emerging waves are either simple waves, or shocks; thus, the wave diagram can take four distinct configurations (Fig. 1).

The strategy of resolution which we follow is frequently employed and known upon the appelation "Godunov iteration" [7, 8]. It consists in giving a value for the pressure in the region between the right and left facing waves: $p^* = p_l^* = p_r^*$ (during the first iteration $p^* = (p_r + p_l)/2$, for example). With the knowledge of this pressure, one determines directly the type of each wave: if the ratio p^*/p_r (or p^*/p_l) is greater than unity, the right (or left) facing wave is a shock wave, else it is a rarefaction wave. To determine the flow parameters behind the waves (r^* and l^* states), one has to know the jump conditions across each type of wave: Riemann invariants for rarefaction waves, jump relations across contact surface, and Hugoniot relations for shock waves. In particular, one has to compute the velocity in each region (v_l^* and v_r^*). As we will see hereafter, it can be shown easily that across the contact surface, pressure and velocity must be constant. So if v_l^* is not equal to v_r^*, that means that the initial value of p^* is not adequate, and one must iterate on p^* until the condition of constant velocity is reached.

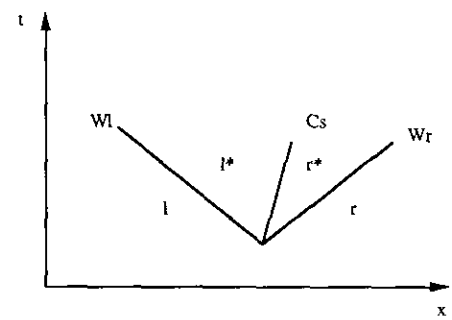

FIG. 1. Representation of Riemann's problem of gas dynamics.

To follow this procedure of resolution, one must know the jump relations across each type of wave. Following Jeffrey [11] one finds:

— Riemann invariants of simple waves facing left or right:

$$\psi_1^{\pm} = s, \qquad \psi_2^{\pm} = v \mp \int^{\rho} \tilde{\rho}^{-1} c(\tilde{\rho}, s)\, d\tilde{\rho} \tag{4}$$

(+, right; −, left). We point out that the integral over ρ has to be evaluated along a constant-entropy curve, and in this fact precisely resides one of the main difficulties.

— Riemann invariants across the contact surface:

$$\psi_1^0 = v, \qquad \psi_2^0 = p. \tag{5}$$

— Relations across the shock: one looks for the state i^*, supposing the state i to be known. The jump relations are:

$$\begin{aligned} \rho_i V_i &= \rho_i^* V_i^* \\ p_i + \rho_i V_i^2 &= p_i^* + \rho_i^* V_i^{*2} \\ h_i + \frac{V_i^2}{2} &= h_i^* + \frac{V_i^{*2}}{2} \end{aligned} \tag{6}$$

with $i = r, l$, $i^* = r^*, l^*$ and $V_i = v_i - U_s$, $V_i^* = v_i^* - U_s$. U_s is the actual propagation velocity of the shock wave, while V is the velocity in a frame of reference bound to the wave. As noted before, the resolution of the RP is considerably simplified if the equation of state is that of a perfect gas. Actually, in Eq. (4) the quadrature is analytic and the system (6) possesses solutions which depend directly upon the shock Mach number; this latter is readily determined from the pressure ratio p_i^*/p_i. On the other hand, if the EOS is such as not to allow using the above facilities, the resolution becomes heavier and more subtle; the trouble stems, essentially, from the evaluation of the Riemann invariant integral, which has to be performed for constant entropy. Let us, e.g., consider the case when one has to determine the flow variables in state l^*, knowing the state l (Fig. 2). The velocity in state l^* is given by

$$v_l^* = v_l - \int_{\rho_l}^{\rho_l^*} \tilde{\rho}^{-1} c(\tilde{\rho}, s)\, d\tilde{\rho}. \tag{7}$$

As we have already pointed out, knowledge of this velocity is essential for the Godunov iteration procedure. The first difficulty resides in finding the limit ρ_l^*. Starting from the known state l, one has to search, along the isentrope passing through l, the state l^*, which is to be found at the intersection of this curve and the isobar $p = p^*$ (where p^* is the pressure which is supposed to be established in the region between the left- and right-facing waves).

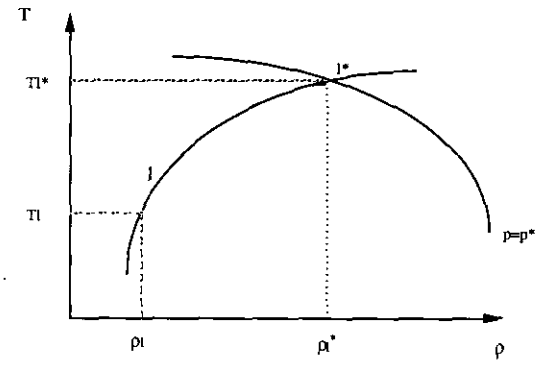

FIG. 2. Intersection between an isobar and an isentrope.

This means that one has to solve the equation $p^* - p(\rho, Ts(\rho)) = 0$, in which the value $Ts(\rho)$ is to be computed, step by step, along the isentrope, with the help of the relation

$$\frac{C_v}{T}\, dT - \frac{1}{\rho^2} \frac{d\rho}{(\partial T/\partial p)_\rho} = 0 \tag{8}$$

which expresses the property $ds = 0$ in the plane (T, ρ). Now, having found ρ_l^*, one may carry out numerically the integration

$$\int_{\rho_l}^{\rho_l^*} \tilde{\rho}^{-1} c(\tilde{\rho}, s)\, d\tilde{\rho} \tag{9}$$

along the isentrope curve. To this purpose, one has to express the sound speed c as a function of certain variables, which should be, in turn, determined by starting from the equation of state. If one has available an EOS of the form $p = p(\rho, T)$, which is true for the equation of state of a perfect gas, the Van der Waals, or the virial equation, then it is convenient to write the speed of sound as

$$c^2 = \left(\frac{\partial p}{\partial \rho}\right)_s = -\frac{C_p}{C_v}\left(\frac{\partial T}{\partial \rho}\right)_p \Big/ \left(\frac{\partial T}{\partial p}\right)_\rho, \tag{10}$$

where C_P and C_V are, respectively, the specific heats at constant pressure and at constant volume, being related by

$$C_p = C_v - \frac{T}{\rho^2} \frac{(\partial \rho/\partial T)_p}{(\partial T/\partial p)_\rho}. \tag{11}$$

The partial derivatives, $(\partial \rho/\partial T)_p$ and $(\partial T/\partial p)_\rho$, appearing in Eqs. (10), (11) are readily calculated with the help of the EOS.

The computation of flow variables behind shock waves poses no special problems. The system of Eqs. (7) can be solved once one knows the expression of the EOS and that of the enthalpy as a function of ρ and T and one is given one

of the variables behind the shock (e.g., p^* or U_s—the shock speed). If an explicit expression for the enthalpy as a function of ρ and T is not available, one may set, in Eq. (7),

$$h_i^* - h_i = \int_{T_i}^{T_i^*} \left(\frac{\partial h}{\partial T}\right)_{\rho=\rho_i^*} dT + \int_{\rho_i}^{\rho_i^*} \left(\frac{\partial h}{\partial \rho}\right)_{T=T_i} d\rho \quad (12)$$

with

$$\left(\frac{\partial h}{\partial T}\right)_\rho = Cv + \frac{1}{\rho(\partial T/\partial p)_\rho},$$
$$\left(\frac{\partial h}{\partial \rho}\right)_T = -\frac{1}{\rho^2}\frac{1+(\rho/T)(\partial T/\partial \rho)_p}{(1/T)(\partial T/\partial p)_\rho}. \quad (13)$$

To summarize, the procedure of computation for solving the RP can be detailed as follows: Set the initial value of p^* ($p^* = (p_r + p_l)/2$, for example). Determine the type of waves travelling to the right and to the left.

If one of these waves is a rarefaction, compute ρ_i^* ($i = r$ or l): Starting from the known state i, follow the isentrope curve with the help of (8) until the condition $p^* - p(\rho, Ts(\rho)) = 0$ is reached. Then compute v_i^* with the help of (7) or (4) expressing the sound speed by (10).

If one of the waves is a shock wave, set an arbitrary value of the shock velocity U_s (for example, the perfect gas shock velocity). Then compute ρ_i^* and V_i^* by the mass and momentum conservation equation of system (6). If the energy equation is not satisfied by the set (ρ_i^*, V_i^*, and p^*) change the initial value of U_s until convergence. If an explicit expression for the enthalpy as a function of ρ and T cannot be derived, use (12) and (13). Compute, thereafter, $v_i^* = V_i^* + U_s$.

If the condition $v_r^* = v_l^*$ is not satisfied, change the initial value of p^*.

Once the Riemann solver has been assembled, it may be incorporated in any numerical method based upon the RP. We have set out, for the test cases to be discussed herein, to use it in the RCM method, which is the method utilising in the most natural way the Riemann problem. The inclusion of the Riemann solver in the RCM, which is a little peculiar because of the random sampling procedure is given in Larini *et al.* [12].

2.1. *Test Problems*

The test case to be investigated is the classical shock-tube problem; in all subsequent numerical comparisons, the overall tube length is 0.4 m, the initial discontinuity is placed at 0.2 m, and the same gas is filling both chambers. In all computations performed with the RCM, the grid chosen consists of 70 points, uniformly distributed along the abscissa.

(a) *Perfect-gas case.* The sole interest of this test case resides in the possibility to check whether the algorithm being incorporated and later to be used for real gases, is working properly. In this case, the shock-tube driver chamber is initially filled with gas at 5000 K and a density of 100 Kg/m^3, while the driven channel contains the same gas, but at 3000 K and 10 Kg/m^3. Results will be presented for the instant $t = 80 \times 10^{-6}$ s.

The equation of state, in this case, reads as $p = \rho RT$, with $R = 231.11$ J/Kg K and

$$\left(\frac{\partial T}{\partial \rho}\right)_P = -\frac{P}{\rho^2 R}$$
$$\left(\frac{\partial T}{\partial P}\right)_\rho = \frac{1}{\rho R}$$
$$Cv = 577{,}8 \text{ J/Kg K}.$$

Results displayed in Diagram 1 show full agreement between the analytic solution and the computed values, thus giving confidence in the correctness of the computational procedure.

(b) *Van der Waals' equation of state.* The shock-tube problem is to be treated here uses the same initial conditions as for the perfect-gas case discussed above. Thus, it will become possible to emphasize the differences in behaviour due to the different equations of state.

Van der Waals' EOS to be used is

$$(P + \alpha\rho^2)(1/\rho - \beta) = \mathrm{RT} \qquad \alpha = 0.138 \text{ (SI)},$$
$$\beta = 3.258 \times 10^{-5} \text{ (SI)}$$
$$R = 231.11 \text{ J/Kg} \cdot \text{K}$$
$$\left(\frac{\partial T}{\partial \rho}\right)_P = \frac{2\alpha\rho - RT/[\rho^2(1/\rho - \beta)^2]}{R/(1/\rho - \beta)}$$
$$\left(\frac{\partial T}{\partial P}\right)_\rho = \frac{(1/\rho - \beta)}{R}$$
$$Cv = 577.8 \text{ J/Kg} \cdot \text{K}.$$

A sufficient condition for convexity of this EOS is $1/\rho > \beta$ and $\alpha > 0$. So this EOS is convex for the present test case.

An analytic solution to the shock-tube problem is not available in this case; therefore the comparison of our results, obtained by applying the above Riemann solver within the random choice method, will be made with those provided by a finite-difference method [14], which does not make use of the resolution of a Riemann problem. This latter method has been applied with grids of 70 and 700 points; only the 700-point grid had to be retained (ten times more

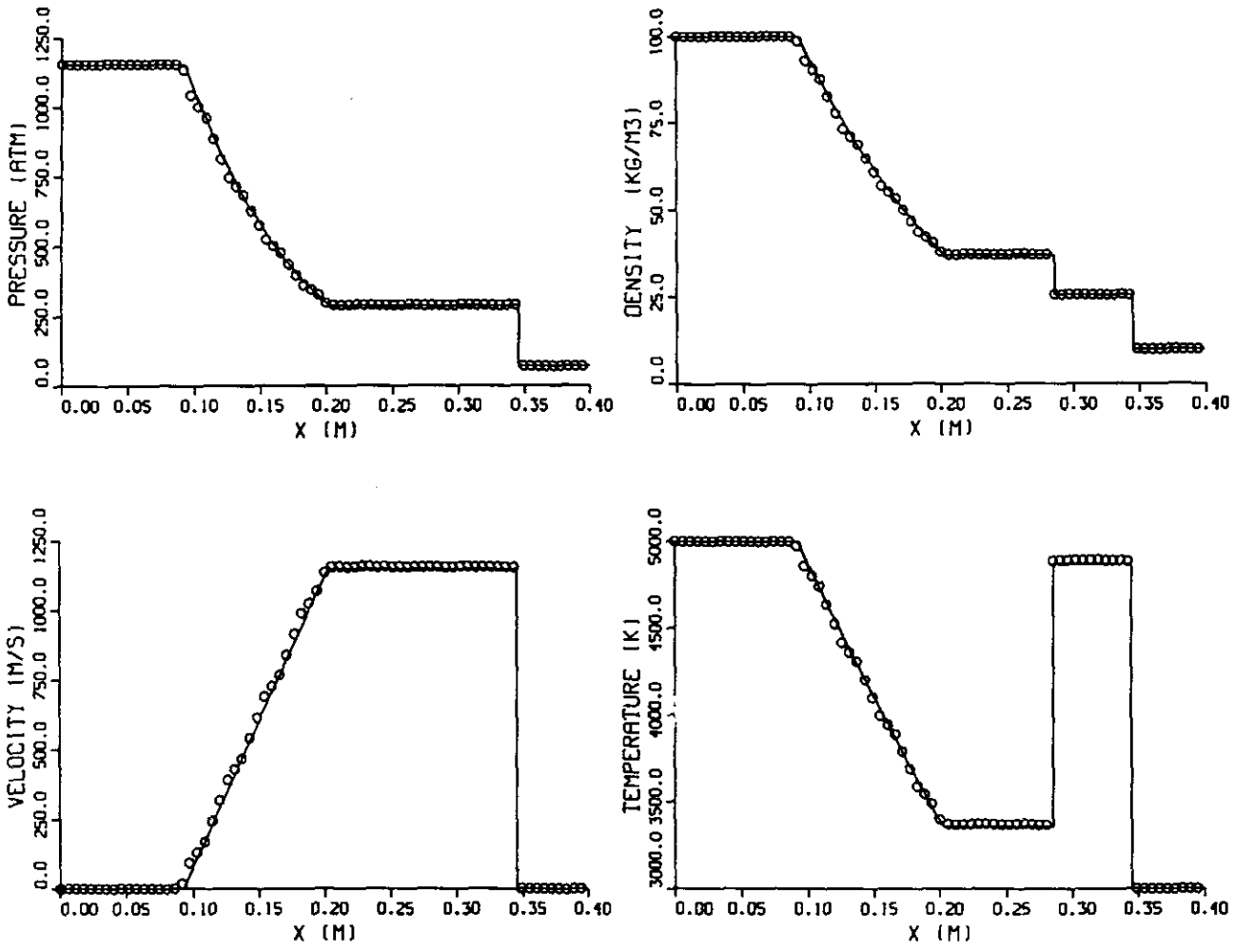

DIAG. 1. Shock tube with perfect gas: ∘, RCM; solid lines, exact solution.

than in the RCM), in order to obtain consistent results. The artificial viscosity coefficients have been chosen following numerical experiments, so as to enhance the capture of discontinuity fronts; thus, an artificial viscosity coefficient of 0.03 was retained for the 700-point grid, while its value for the 70-point grid has been set at 0.003.

Comparing the values of the pressures and the positions of the shock and contact surfaces in Diagrams 1 and 2, one may assess the differences brought about by the use of the Van der Waals EOS, in contrast with the perfect-gas case.

(c) *Fifth-order virial equation of state.* The same shock-tube test problem will now be reconsidered, but under extreme initial conditions, rendered possible by the adoption of this EOS: namely, in the driver chamber, an initial temperature of 5000 K and initial density of 1800 Kg/m^3; while in the driven channel one starts with 3000 K and 100 Kg/m^3; results are presented for $t = 24 \times 10^{-6}$ s.

The particular EOS to be employed has been developed by Heuzé [10], especially for the study of detonation products of highly energetic explosives. It has been successfully applied to numerous problems in detonation theory [1, 2] and to the study of the deflagration–detonation transition [18]. Its expression is

$$p = \rho RT\sigma(x) \qquad \text{with} \quad \sigma(x) = 1 + x + 0.625x^2 + 0.287x^3 - 0.093x^4 + 0.0014x^5,$$

where $x = \rho\Omega/T^{0.33}$ while Ω depends upon the gas composition and the covolume of its constituents (for the explosive studied here $\Omega = 18.66 \times 10^{-3}$ (SI),

$$\left(\frac{\partial T}{\partial \rho}\right)_P = \frac{1 A_V}{\rho^2 A_T}$$

$$\left(\frac{\partial T}{\partial P}\right)_\rho = \frac{1}{A_T}$$

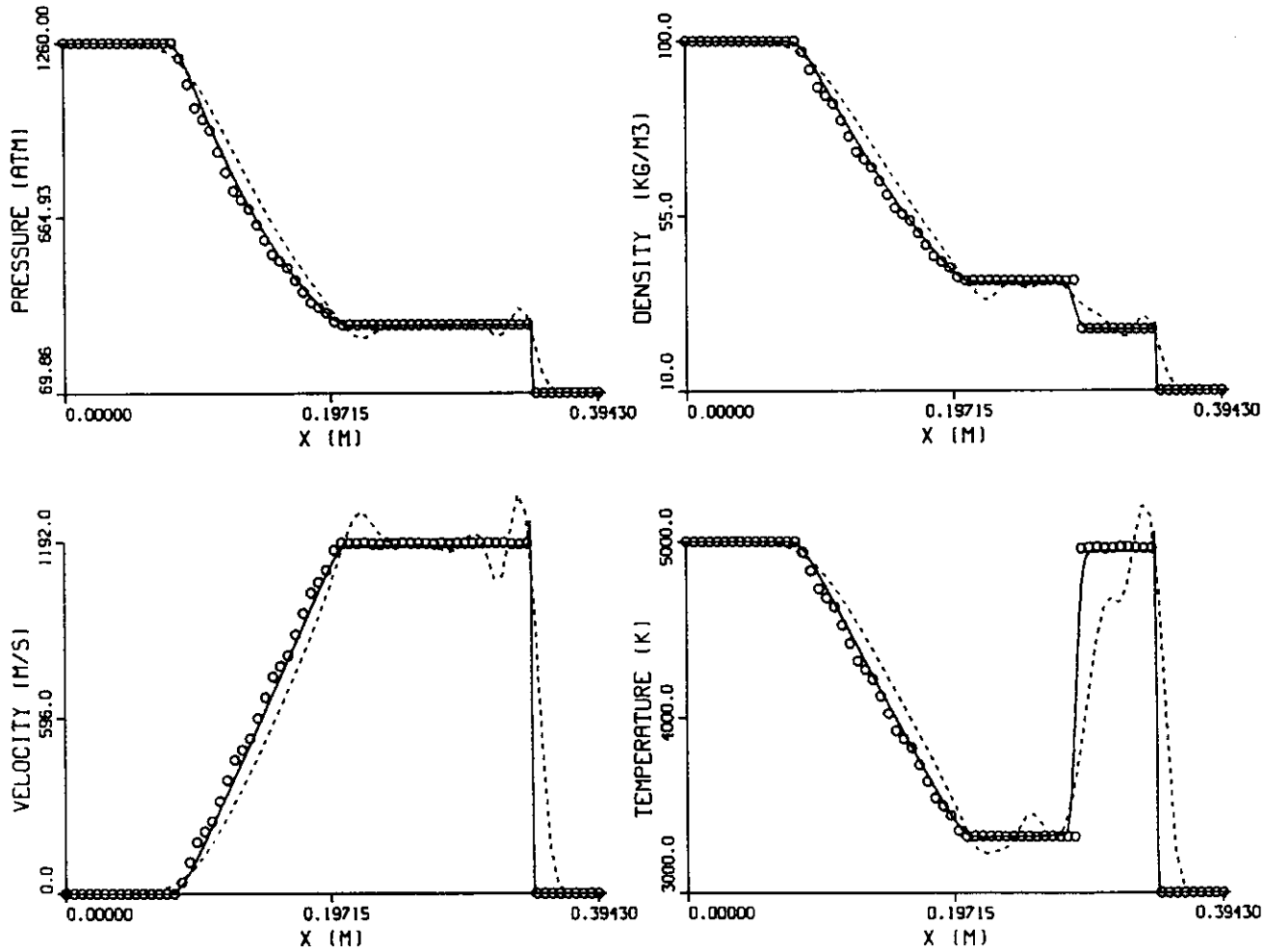

DIAG. 2. Shock-tube with Van der Waals EOS. Comparison of RCM-finite-differences: ∘, RCM; solid lines, finite-differences, 700 points; dotted lines, finite-differences, 70 points.

with

$$A_T = \rho R\left[\sigma(x) - 0.33\,\frac{\rho\Omega}{T^{0.33}}\,\frac{d\sigma}{dx}\right],$$

$$A_V = -\rho R\left[\rho T\sigma(x) + \rho^2 T^{0.67}\Omega\,\frac{d\sigma}{dx}\right].$$

C_V is derived here from Helmholtz's free-energy [10] and thermochemical data (JANAF tables). The enthalpy is directly deduced from the equation of state; denoting by $E^\circ(T)$ the "perfect-gas" part of the internal energy, one has

$$h(\rho, T) = E^\circ(T) + \frac{RT}{3}(\sigma(x) - 1) + \frac{p(\rho, T)}{\rho}.$$

This EOS is always convex in its domain of validity: $1\ \text{Kg/m}^3 < \rho < 1800\ \text{Kg/m}^3$ and $300\ \text{K} < T < 10{,}000\ \text{K}$.

In the two real-gas cases examined, the superiority of the RCM is obvious, by comparison with the finite-difference method, even when the number of points differs by a factor of 10 (see, in particular, the capture of the contact surface, Diagram 3); nevertheless, referring to the required computer time, the higher accuracy of the RCM appears as very costly:

	CPU (seconds on an IBM 3090)	
	Van der Waals	Fifth-order virial
finite-differences, 700 points	14.5	23
RCM 70 points	40	91

These findings provided the motivation for the following analysis, in which certain assumptions will be put forward, in order to ease the numerical computation.

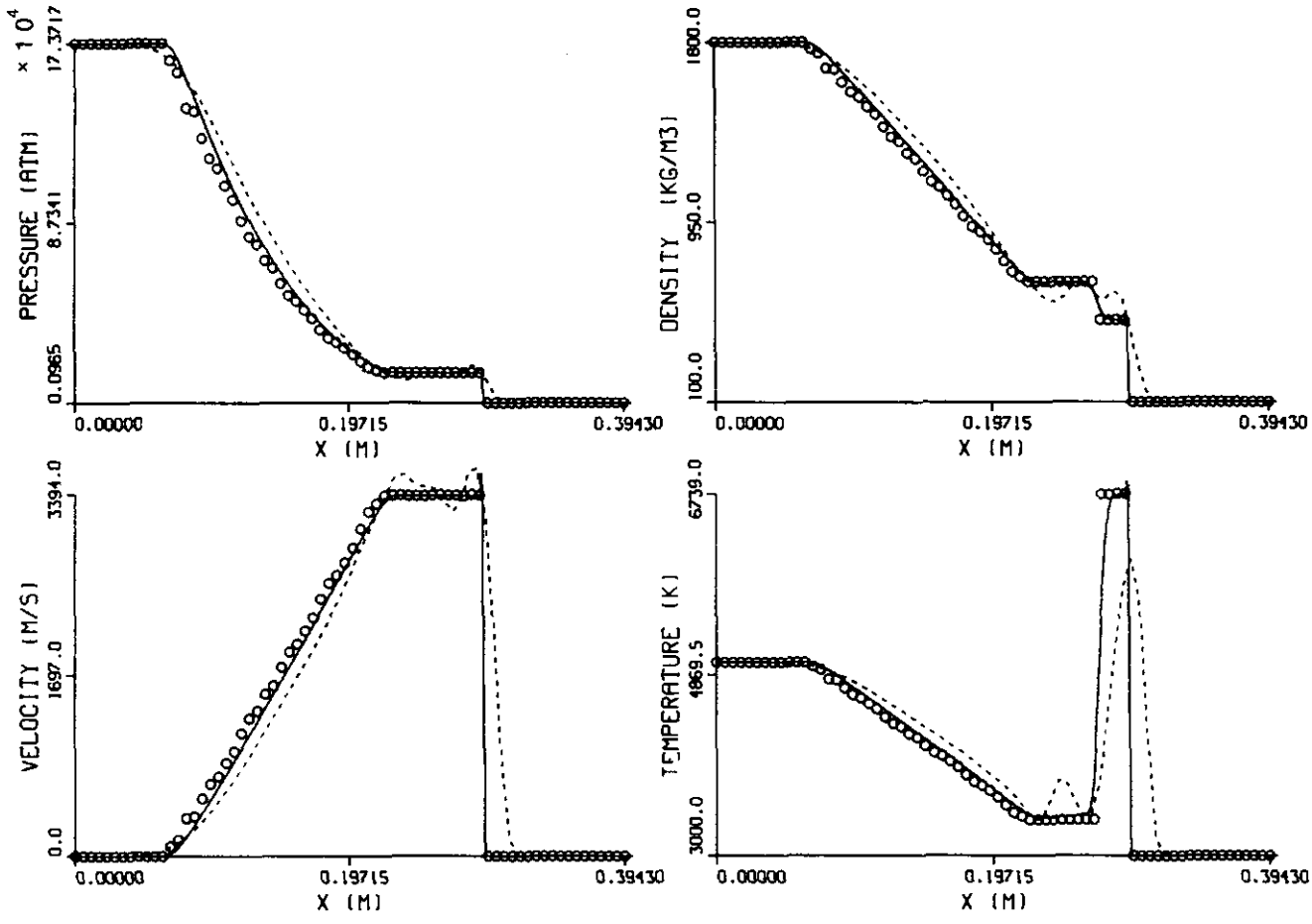

DIAG. 3. Shock-tube with a gas obeying a fifth-order virial equation of state: ∘, RCM; solid lines, finite differences, 700 points; dotted lines, finite differences, 70 points.

3. APPROXIMATE SOLUTION OF THE EXACT RIEMANN PROBLEM FOR A REAL GAS

In this section, an approximate solution procedure will be developed for the exact Riemann problem; the aim is to set up a more competitive method, in terms of CPU time, than the exact method discussed above. The improvement is arrived at by introducing certain assumptions in the computation of simple waves. Results to be shown will again be obtained after implementing the solver in the RCM.

3.1. *Thermodynamic Foundations*

Davis [22] and later Menikoff and Plohr [15] have emphasized the interest of using non-dimensional parameters for characterizing the thermodynamic state of the fluid. Within our work we shall make use of two such parameters, as introduced by Menikoff and Plohr [15],

$$\gamma = \frac{v}{p}\left(\frac{\partial^2 e}{\partial v^2}\right)_s \tag{14}$$

$$\Gamma = -\frac{v}{T}\left(\frac{\partial^2 e}{\partial s\, \partial v}\right). \tag{15}$$

Where $v = 1/\rho$, γ is the adiabatic exponent, while Γ is Gruneisen's coefficient. These two parameters are precisely those which will serve to develop the approximate resolution method. First, regarding the adiabatic coefficient, it is easily proved that it can be written as

$$\gamma = \frac{\rho}{p}\left(\frac{\partial p}{\partial \rho}\right)_s \tag{16}$$

or, further, after some thermodynamic transforms,

$$\gamma = -\frac{\rho}{p}\frac{Cp(\partial T/\partial \rho)_p}{Cv(\partial T/\partial p)_\rho}. \tag{17}$$

Equation (17) is particularily interesting since, if one has an EOS of the form $p = p(\rho, T)$, it becomes easy to express the adiabatic exponent in terms of ρ and T. In the particular case when the EOS is chosen to be that of a perfect gas, one recovers, for the adiabatic coefficient, $\gamma = \gamma_{pg} = Cp/Cv$.

On the other hand, Gruneisen's coefficient, as defined by Eq. (15), can be written in a simpler form,

$$\Gamma = \frac{\rho}{T}\left(\frac{\partial T}{\partial \rho}\right)_s \tag{18}$$

or, even more practically,

$$\Gamma = \frac{1}{\rho C v}\frac{1}{(\partial T/\partial p)_\rho}. \tag{19}$$

This latest equation expresses directly Γ as function of ρ and T. In the particular case of the perfect-gas EOS, one has

$$\Gamma = \Gamma_{pg} = \frac{Cp}{Cv} - 1 = \gamma_{pg} - 1.$$

Remarks. In order to compute γ and Γ with the help of Eqs. (17) and (19), one has to know the quantities $(\partial T/\partial \rho)_p$ and $(\partial T/\partial p)_\rho$ and, therefore, to be given an equation of state. One has to know also eigher C_p or C_v, the specific heats at constant pressure and volume, which are related through Eq. (11). In the particular case of the perfect-gas EOS, one recovers the formula $Cp = Cv + R$. On the other hand, the speed of sound, which has been defined by Eq. (2), can now be written, making use of Eq. (16), whichever is the EOS to be adopted:

$$c^2 = \gamma p/\rho. \tag{20}$$

3.2. *Approximations along an Isentrope*

Equations (16) and (18) may be written along an isentrope curve, as

$$dp/p - \gamma\, d\rho/\rho = 0 \tag{21}$$

$$dT/T - \Gamma\, d\rho/\rho = 0, \tag{22}$$

and, from these, one can derive another relation, valid along an isentrope,

$$dT/T - \Gamma/\gamma\, dp/p = 0. \tag{23}$$

If Eqs. (21), (22), and (23) are integrated along an isentrope, between two states, defined by p_i, ρ_i, T_i and p_i^*, ρ_i^*, T_i^*, which are sufficiently near, in order to allow considering that γ and Γ are constant along the isentrope connecting these states, it follows that

$$\frac{p_i^*}{p_i} = \left(\frac{\rho_i^*}{\rho_i}\right)^\gamma \tag{24}$$

$$\frac{T_i^*}{T_i} = \left(\frac{\rho_i^*}{\rho_i}\right)^\Gamma \tag{25}$$

$$\frac{T_i^*}{T_i} = \left(\frac{p_i^*}{p_i}\right)^{\Gamma/\gamma}. \tag{26}$$

If, however, the assumption of constant γ and Γ is not fully justified, since the two states i^* and i are not sufficiently close to each other, one may still use Eqs. (24), (25), and (26), taking, as approximate values for γ and Γ, their mean values

$$\bar{\gamma} = 0.5(\gamma(\rho_i, T_i) + \gamma(\rho_i^*, T_i^*)) \tag{27}$$

$$\bar{\Gamma} = 0.5(\Gamma(\rho_i, T_i) + \Gamma(\rho_i^*, T_i^*)). \tag{28}$$

Use of Eqs. (27) and (28) might require iteration.

3.3. *Approximate Resolution of the Riemann Problem*

The simplifying assumptions which will be brought into the solution of the RP concern the computation of simple waves. The quantities defined by Eq. (5) are Riemann invariants which, for a left-facing wave, lead to the relation

$$v_l^* = v_l - \int_{\rho_l}^{\rho_l^*} \tilde{\rho}^{-1} c(\tilde{\rho}, s)\, d\tilde{\rho} \tag{29}$$

and, for a right-facing wave, lead to

$$v_r^* = v_r + \int_{\rho_r}^{\rho_r^*} \tilde{\rho}^{-1} c(\tilde{\rho}, s)\, d\tilde{\rho}. \tag{30}$$

Here, the states l and r are supposed known, and one has to find the states l^* and r^* that fulfill Eqs. (29) and (30). Using Eq. (20), one may eliminate the sound speed between Eqs. (29) and (30). Let us consider, e.g., a left-facing wave. Suppose that the states l and l^* are sufficiently close to each other and, as the integration has to be carried out along an isentrope, that one may use Eq. (24) and perform an analytic quadrature. It follows that

$$I_l = \int_{\rho_l}^{\rho_l^*} \tilde{\rho}^{-1} c(\tilde{\rho}, s)\, d\tilde{\rho} = \frac{2}{\gamma_l - 1} c_l \left[\left(\frac{\rho_l^*}{\rho_l}\right)^{(\gamma_l - 1)/2} - 1\right], \tag{31}$$

where $\gamma_l = \gamma(\rho_l, T_l)$.

Within the same assumptions one obtains, for the right-facing wave,

$$I_r = \frac{2}{\gamma_r - 1} c_r \left[\left(\frac{\rho_r^*}{\rho_r}\right)^{(\gamma_r - 1)/2} - 1\right]. \tag{32}$$

Keeping into account Eqs. (31), (32), and (24), relations (29) and (30) become

$$v_l^* = v_l - \frac{2}{\gamma_l - 1} c_l \left[\left(\frac{p_l^*}{p_l} \right)^{(\gamma_l - 1)/2\gamma_l} - 1 \right] \tag{33}$$

$$v_r^* = v_r - \frac{2}{\gamma_r - 1} c_r \left[\left(\frac{p_r^*}{p_r} \right)^{(\gamma_r - 1)/2\gamma_r} - 1 \right]. \tag{34}$$

The computation of shock waves remains, on the other hand, unchanged (see Section 2).

Remarks. If the states l and, respectively, r, are not sufficiently close to the states l^* (or r^*), by extension of what has already been presented in Section 3.2, one may still use Eqs. (33) and (34), after replacing γ_l (and, respectively, γ_r) by

$$\bar{\gamma}_l = \tfrac{1}{2}(\gamma_l + \gamma_l^*) \qquad (\text{resp. } \bar{\gamma}_r = \tfrac{1}{2}(\gamma_r + \gamma_r^*)).$$

On the other hand, the iterative solution of the RP requires that the value of p^*, the pressure prevailing between the left- and right-facing waves be given. The choice $p^* = (p_r + p_l)/2$ often proves itself to be inaccurate. A good guess for the initial value p^* can be obtained by assuming that the left- and right-waves are simple waves. Writing that $v = v_l^* = v_r^*$ and that $p^* = \bar{p}l^* = p_r^*$ in Eqs. (33) and (34) one finally finds

$$P^* = \left[\frac{c_l + c_r + ((\gamma - 1)/2)(v_l - v_r)}{\dfrac{c_l}{P_l^{(\gamma-1)/2}} + \dfrac{c_r}{P_r^{(\gamma-1)/2}}} \right] \qquad \text{with} \quad \gamma = \gamma_r + \gamma_l/2 \tag{35}$$

3.4. *Test Problems*

The test cases are computed using the same conditions as in the preceding section; thus, one is able to compare the differences in accuracy and computing times.

(a) Van der Waals' equation of state. The agreement here is excellent, with indistinguishible differences between the exact and approximate solvers (Diagram 4).

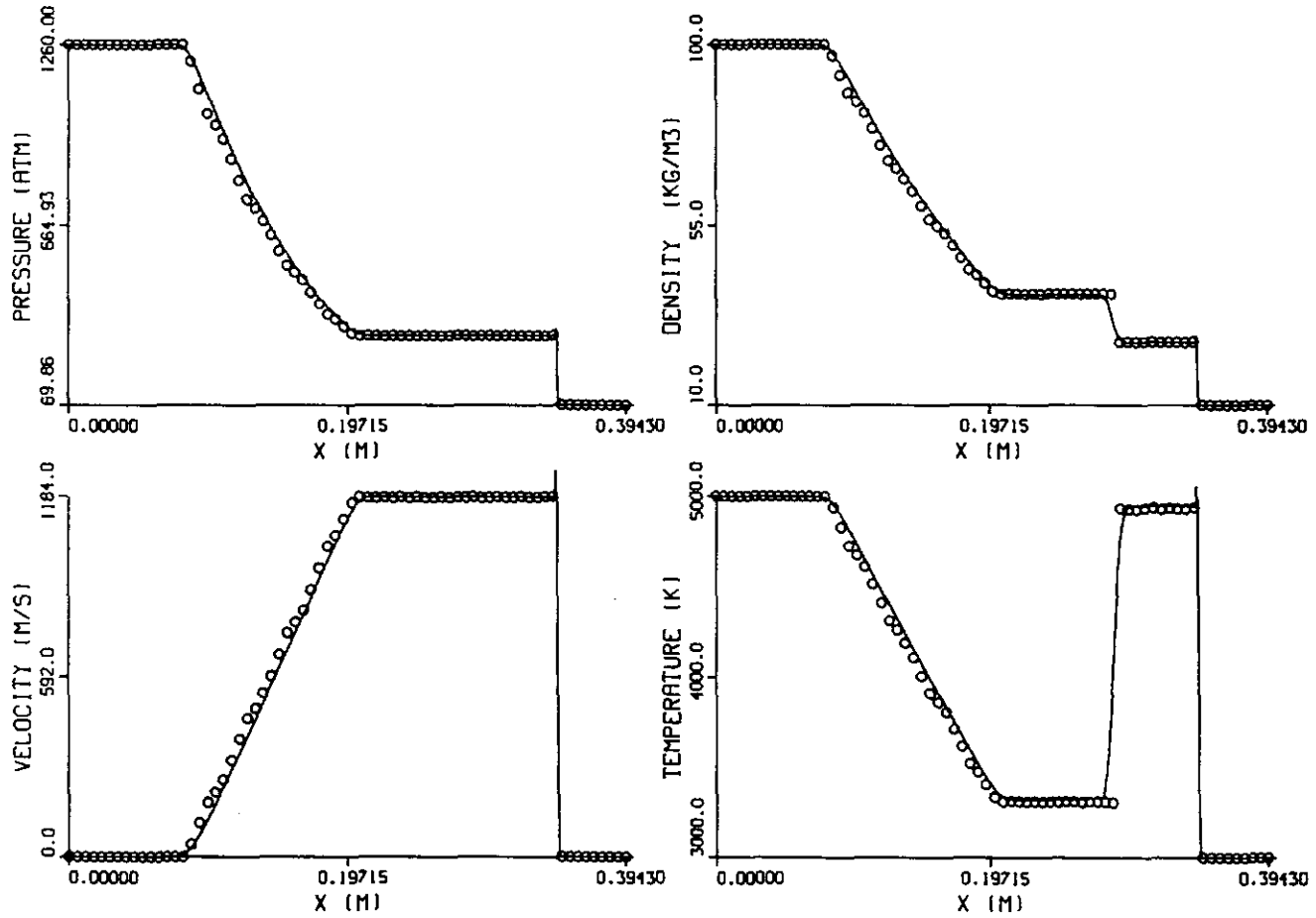

DIAG. 4. Shock-tube with Van der Waals gas. Comparison between RCM (approximate solver) and finite-differences: ∘, RCM; solid lines, finite differences, 700 points.

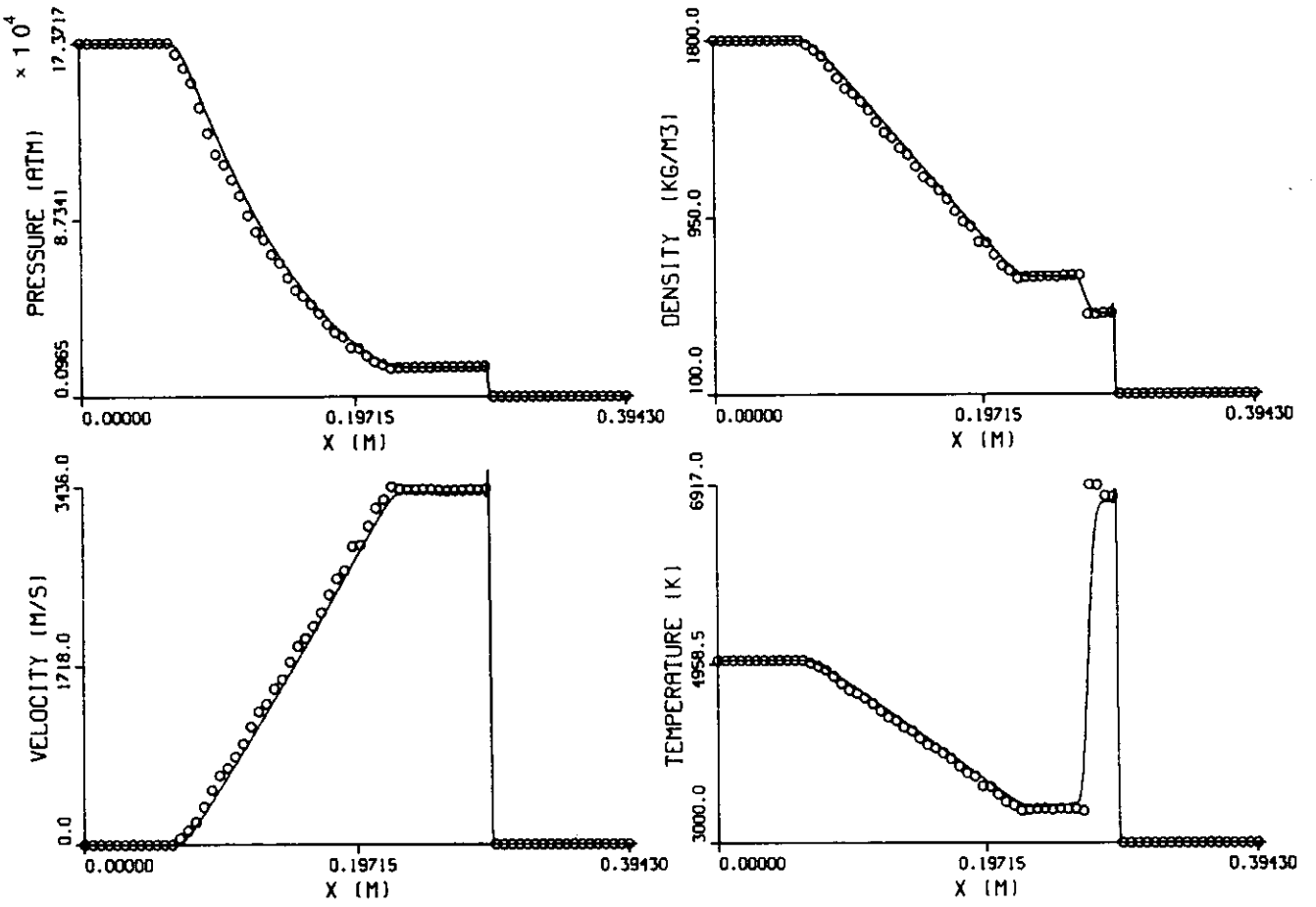

DIAG. 5. Shock-tube with fifth-order virial equation of state (approximate solver): ∘, RCM; solid lines, finite-differences, 700 poins.

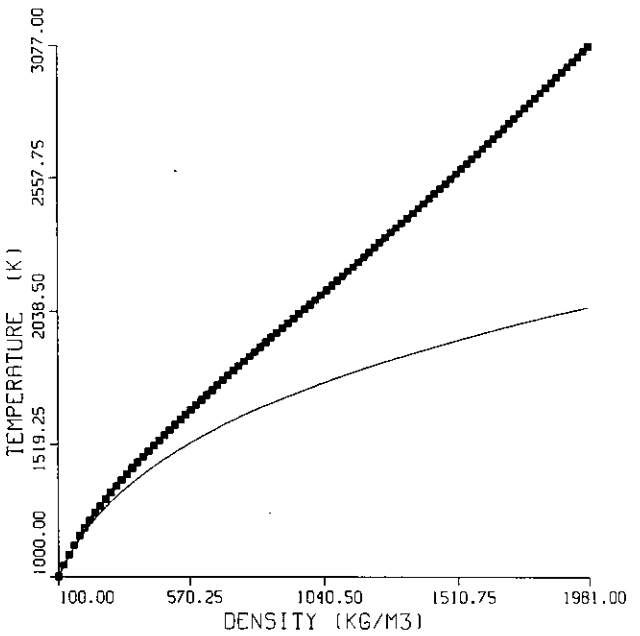

FIG. 3. Exact (■) and approximate (solid lines) isentropes, starting from the driven channel conditions and reaching the driver chamber density, for the fifth-order virial EOS.

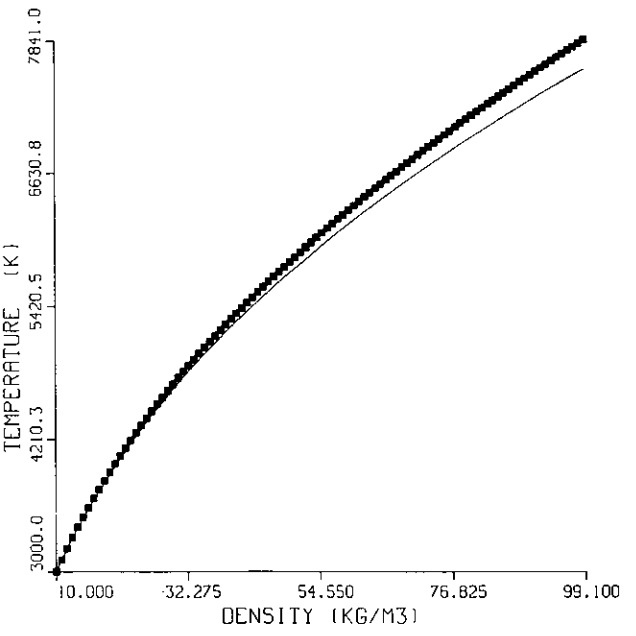

FIG. 4. Exact (■) and approximate (solid lines) isentropes, starting from the driven channel conditions and reaching the driver chamber density, for the Van der Waals EOS.

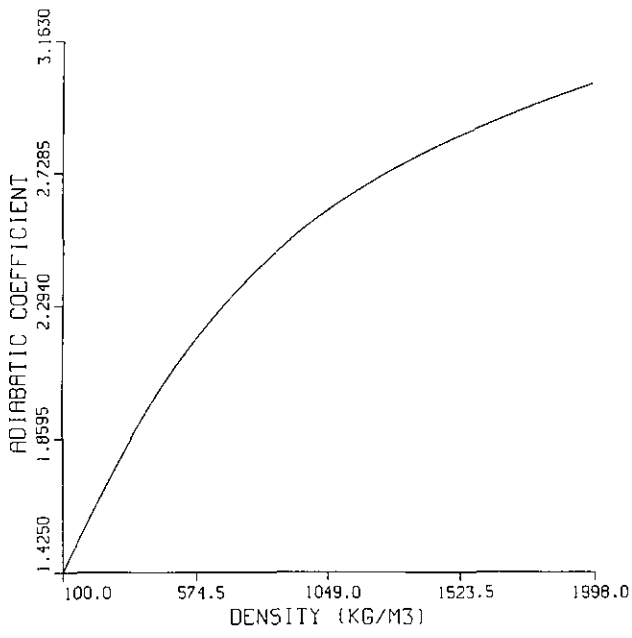

FIG. 5. Variations of γ along the exact isentrope, starting from the driven channel conditions and reaching the driver chamber density, for the fifth-order virial EOS.

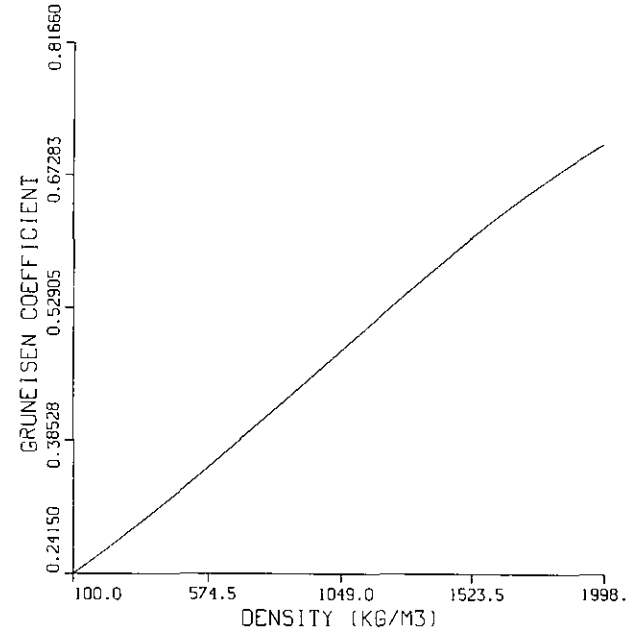

FIG. 6. Variations of Γ along the exact isentrope, starting from the driven channel conditions and reaching the driver chamber density, for the fifth-order virial EOS.

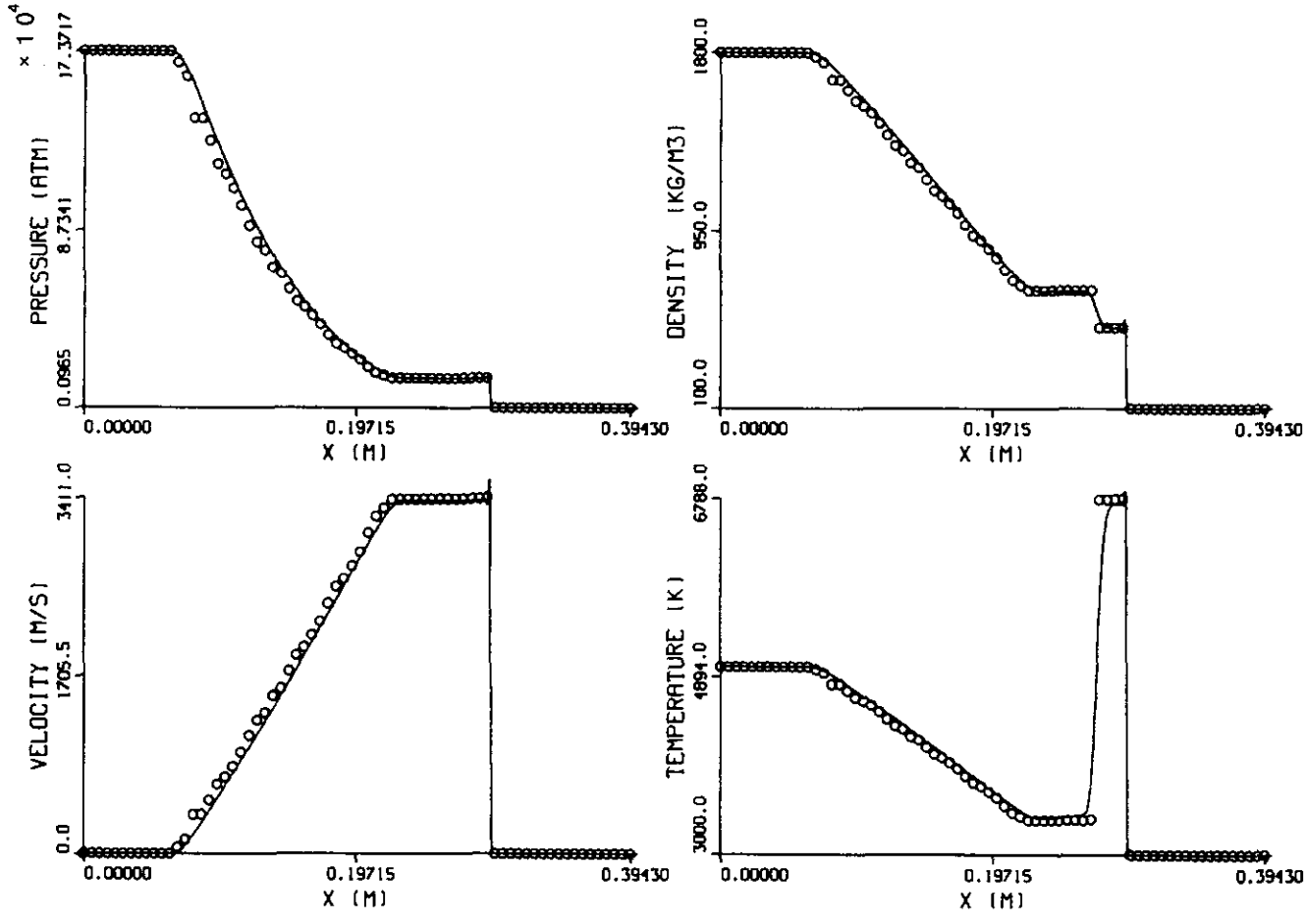

DIAG. 6. Shock-tube with fifth-order virial EOS (exact and approximate solvers): ∘, RCM; solid lines, finite-differences, 700 points.

(b) Fifth-order virial equation of state. This test case allows us to consider extreme thermodynamic conditions. A slight disagreement is observed (Diagram 5), essentially in the computation of the temperatures on the two sides of the contact surface. This is explained by the excessive discrepancies between the state l, in the driver chamber, and the state l^*, whereby the assumption of constant (or mean) γ and Γ fails when the resolution of the first Riemann problems is undertaken. This can be pointed out by plotting exact and approximate isentropes (Fig. 3), starting from the conditions of the low pressure chamber and reaching the density of the high pressure chamber. These isentropes are found using relation (8) for the exact isentrope and (25) for the approximate one, taking for Γ the value in the low pressure chamber.

By contrast, one can see in the case of Van der Waals EOS that the discrepancy between exact and approximate isentropes is less important (Fig. 4).

When the assumption of a constant Γ and γ is no longer valid (in the case of the virial EOS) one must use the exact Riemann solver. If we plot variations of γ and Γ along the exact isentrope (Figs. 5 and 6) one can devise a criterion for the use of the exact or approximate solver.

For the present EOS, so long as the ratio Γ_r/Γ_l is comprised between 0.7 and 1.4, the approximate Riemann solver is sufficiently accurate; else one must use the exact solver. This situation occurs for the present calculation only during the first three time steps. Use of the exact solver for the first time-steps permits one to compute several points (at least two) within the expansion wave and so to dispose of states lying sufficiently close to each other for the subsequent computation using the approximate solver. Excellent results are then obtained, without being too costly in terms of CPU time (Diagram 6).

The solver thus set up is now competitive as to CPU time in all cases, and it is highly accurate.

	CPU (seconds on an IBM 3090)	
	Van der Waals	Fifth-order virial
Finite-differences, 700 points	14.5	23
RCM, 70 points (approximate)	4.2	6.2
RCM, 70 points (mixed method)		7.9

4. CONCLUSIONS

Two methods for the resolution of the exact Riemann problem, in the case of a real gas, have been put forward. The first furnishes an exact solution to the exact RP, but it is difficult to implement and costly in CPU time. The second method provides an approximate solution to the exact RP, which is much faster and easier to set up. The simplification stems from a set of assumptions which greatly simplify the computation of simple waves. In most cases of practical interest, the approximate solver gives excellent results and may, therefore, be embedded into multi-dimensional codes which are based upon the use of the Riemann problem. It may also be used with any other method for the computation of boundary points.

REFERENCES

1. P. Bauer, H. N. Presles, O. Heuzé, and C. Brochet, *Combust. Flame* **64**, 113 (1986).
2. P. Bauer, P. Vidal, N. Manson, and O. Heuzé, *Prog. Astronaut. Aeronaut.* **114**, 64 (1988).
3. P. Colella and H. M. Glaz, *J. Comput. Phys.* **59**, 264 (1985).
4. A. J. Chorin, *J. Comput. Phys.* **22**, 517 (1976).
5. P. Glaister, *J. Comput. Phys.* **74**, 382 (1988).
6. J. Glimm, *Commun. Pure Appl. Math.* **18**, 697 (1965).
7. S. K. Godunov, *Math. Sb.* **47**, 357 (1959).
8. J. Gottlieb, "Lecture Course Note on Random Choice Method for Solving One-Dimensional Unsteady Flows in Ducts, Shock Tubes and Blast Wave Simulators," presented at AC-Lab., Spiez, Switzerland, May 21–30, 1986 (unpublished).
9. J. Gottlieb and C. P. T. Groth, *J. Comput. Phys.* **78**, 437 (1988).
10. O. Heuzé, *Phys. Rev. A* **34**(1), 428 (1986).
11. A. Jeffrey, *Quasilinear Hyperbolic Systems and Waves*, Research Notes in Mathematics, Pitman, New York, 1976.
12. M. Larini, R. Saurel, and J. C. Loraud, *Shock Waves* **2**, 225 (1992).
13. M. S. Liou, B. Van Leer, and J. S. Shuen, *J. Comput. Phys.* **87**, 1 (1990).
14. R. W. MacCormack, AIAA Paper 69-353, 1969.
15. R. Menikoff and B. J. Plohr, *Rev. Modern Phys.* **61**, No. 1 (1989).
16. B. J. Plohr, *AIAA J.* **26**(4), 470 (1988).
17. P. L. Roe, *J. Comput. Phys.* **43**, 357 (1981).
18. R. Saurel, M. Larini, and J. C. Loraud, *Shock Waves* **2**, 19 (1992).
19. E. F. Toro, *Int. J. Numer. Methods Fluids* **9**, 1145 (1989).
20. B. Van Leer, *J. Comput. Phys.* **32**, 101 (1979).
21. M. Vinokur and J. L. Montagné, *J. Comput. Phys.* **89**, 276 (1990).
22. Davis, *in* Eighth Int. Symp. on Detonation, edited by Short (Naval Surface Weapons Center, White Oak, Silver Springs, MD), p. 785, 1985.